

Contents list available at CBIORE journal website

International Journal of Renewable Energy Development

Journal homepage: https://ijred.cbiore.id



Research Article

Formulation of Nb-doped ZnO nanoparticles towards improved photo conversion performance via luminescent down-shifting of the incident spectrum

Yaumee Natasha Jusoh^a, Omsri Vinasha Aliyaselvam^a, Nurul Aliyah Zainal^a, Ahmad Nizamuddin Mustafa^{a,b}, Ahmad Syahiman Mohd Shah^a, Fauziyah Salehuddin^a, Faiz Arith^a

Abstract. The quest for optimal solar energy utilization has prompted an investigation into materials and techniques, establishing luminescent down shifting (LDS). This method converts short-wavelength photons into longer wavelengths thus expanding the range of absorption. This may further enhance the efficiency of solar cell power conversion. Herein, the Zinc Oxide (ZnO) nanoparticle is introduced as a promising candidate for LDS, mainly due to its ability to convert light effectively and cost-savvy. This research delves into enhancing Niobium (Nb) doped ZnO particles that exhibit photoluminescent characteristics to improve energy conversion efficiency. The synthesis of 1% mol of Nb-doped ZnO nanoparticles on indium tin oxide (ITO) films was achieved using a low-temperature hydrothermal technique, varying the growth duration. Extensive analysis using XRD, SEM, and UV-Vis spectroscopy revealed that the optimal outcomes were achieved with an 8-hour growing period. The analysis revealed a hexagonal wurtzite crystal structure, characterized by prominent peaks on the (111) plane and a crystallite size of 37.18 nm. A morphology study indicated that the ZnO nanorods exhibited a randomly uniform oriented arrangement and a densely formed structure measuring $0.77 \pm 0.02 \, \mu m$. The samples exhibited promising optoelectronic properties based on the analysis, such as a characteristic bandgap of $3.35 \, eV$, a transmittance of 46.54%, and an absorbance of $0.33 \, a.u$. Furthermore, the electrical conductivity of the Nb-doped ZnO films was recorded at $1.62 \, m\Omega^{-1}$. These findings suggest that controlling the Nb growth offers a promising avenue for optimizing the performance of Nb:ZnO nanoparticles for advanced solar energy conversion applications.

Keywords: Niobium, Zinc oxide nanoparticles, Down-shifting, Hydrothermal



@ The author(s). Published by CBIORE. This is an open access article under the CC BY-SA license (http://creativecommons.org/licenses/by-sa/4.0/).

Received: 13th Dec 2024; Revised: 19th Feb 2025; Accepted: 13th March 2025; Available online: 20th March 2025

1. Introduction

Solar energy is an important component of renewable energy sources, and its technology has developed rapidly and shown the most promising progress. From that, perovskite solar cells have demonstrated remarkable progress, achieving a power conversion efficiency (PCE) of 26.1% in a relatively short timeframe (Alias et al., 2022). This surpasses the development pace of silicon solar cells, highlighting the potential of perovskites as a leading renewable energy technology (Alias et al., 2022). Ongoing research in component optimization, interface engineering, additive engineering, and functional layer development continues to drive advancements in perovskite solar cells (Aliyaselvam et al., 2022; Hammad et al., 2021; Jalaludin et al., 2025; Wahab et al., 2024). This study explores the integration of luminescent down-shifting (LDS) layers into perovskite solar cells, a strategy that has shown promise in enhancing light-harvesting capabilities in silicon solar cells.

Indium Tin Oxide (ITO) thin films are widely used as transparent conductive oxides due to their low electrical resistance. Flexible substrates like ITO-coated polyethylene naphthalate (PEN) and ITO-coated polyethylene terephthalate (PET) are popular choices for perovskite solar cells (PSCs), combining affordability, lightweight design, and flexibility (Eswar *et al.*, 2023).

Zinc Oxide (ZnO) is an II-VI semiconductor known for its wide bandgap, approximately 3.37 eV and high exciton binding energy of around 60 meV (Nguyen *et al.*, 2022)(Alias *et al.*, 2022). These properties are common in binary compounds. Niobium (Nb) is a valuable element with strong mechanical, thermal, and electronic properties. Doping ZnO with Nb is significant because it introduces additional electrons for electrical conduction, due to the valence difference between Zn²⁺ and Nb⁵⁺ (Cantarella *et al.*, 2024).

Numerous methods exist for synthesizing new materials (Jafari *et al.*, 2018). Sol-gel (Alias *et al.*, 2022), hydrothermal, (Çolak *et al.*, 2023)(Jusoh *et al.*, 2024), spray-pyrolysis (Khalil *et*

^aFaculty of Electronic and Computer Engineering and Technology Hang Tuah Jaya, 76100, University Technical Malaysia Malacca, Malaysia

^bDepartment of Materials, Faculty of Engineering, Imperial College London, London SW7 2AZ, United Kingdom

^cDepartment of Electrical Engineering, College of Engineering, University Malaysia Pahang, Lebuhraya Tun Razak, Gambang, Pahang, Kuantan, 26300, Malaysia

al., 2014) and thermal decomposition (Gerbreders et al., 2020). are common techniques for producing doped ZnO particles. The hydrothermal method is particularly advantageous for ZnO synthesis due to its simplicity, cost-effectiveness, low-temperature processing, scalability, and high yield. While many studies have focused on this method, the goal is to achieve lower temperatures and faster synthesis times (Mustaffa et al., 2022).

An extensive study has been carried out on the impact of dopants on ZnO thin sheet films. Integrating transition metal oxide dopants, including manganese (Mn) (Chvostová et al., 2011), chromium (Cr) (Fu et al., 2013), cobalt (Co) (Khare et al., 2006), iron (Fe) (Hammad et al., 2021)(Hammad & Abdel-Wahab, 2021) (Hammad et al., 2021), and copper (Cu) (Guzman et al., 2004), , into the ZnO lattice improves its magnetic characteristics. These substances, referred to as diluted magnetic semiconductors, have significant use in spintronic applications. The increase in electrical conductivity of zinc oxide (ZnO) by doping it with titanium (Ti) is ascribed to the 30% reduction in radius of the Ti⁴⁺ ion compared to the Zn²⁺ ion (Hammad et al., 2021; Lu et al., 2004; Ma et al., 2011). In contrast, the incorporation of dopants such as aluminium (Al) (Bagiyev et al., 2015), magnesium (Mg) (Dhawan et al., 2019), tin (Sn) (Özgür et al., 2019), and indium (In) (Kotlyarchuk et al., 2005), leads to the formation of ZnO films that demonstrate both transparency and excellent conductivity, therefore rendering them appropriate for use as transparent conductive oxides (TCO). In addition, rare-earth elements like neodymium (Nd) and terbium (Tb) improve both clarity and conductivity, as well as luminosity (El Fakir et al., 2017). ZnO thin films doped with lanthanum (La) (Pascariu et al., 2019) are known for their photocatalytic characteristics.

Although numerous LDS materials have been studied for perovskite solar cells, the potential of Nb-doped ZnO remains unknown in this context. This highlights a notable deficiency in existing research, as Nb-doped ZnO showcases encouraging characteristics, including increased transparency, which facilitates greater light penetration into the active layer (Sanz et al., 2006), enhanced interaction with the organic active layer (Naz et al., 2018), and greater electron extraction (Naz et al., 2018), potentially resulting in enhanced device performance. Moreover, the ideal growth conditions for attaining effective down-conversion in the realm of perovskite solar cells are still not fully understood. This study seeks to fill important gaps by synthesizing Nb-doped ZnO nanoparticles with different growth durations and investigating the relationship between their structural and optical properties as a luminescent downshift layer.

2. Experimental Procedure

2.1 Materials

Zinc acetate, Zn (CH $_3$ CO $_2$) $_2$ (>=98%), Hexamethylenetetramine (CH $_2$) $_6$ N $_4$ (99%), Sodium hydroxide, NaOH (\geq 97.0 %) and Niobium pentoxide, Nb $_2$ O $_5$ (99.9%) were purchased from QreC, Scharlab, Merck, Sigma, respectively. All chemicals were utilized as received, with no further purification of reagents conducted.

2.2 Synthesis

Nb-doped ZnO powders were obtained using Zinc acetate dihydrate(Zn(CH₃COO)₂:2H₂O,≥98%),hexamethylenetetramine

 $(C_6H_{12}N_4, 99\%)$, sodium hydroxide (NaOH, \geq 97.0%), and niobium pentoxide (Nb₂O₅, 99.9%) were obtained from QreC, Scharlab, Merck, and Sigma-Aldrich, respectively. All chemicals were directly utilised as received without any additional purification as illustrated in Figure 1. For substrate preparation, the films coated with ITO were cut into small squares with dimensions of 2.0 cm \times 1.5 cm. The substrates underwent a thorough cleaning process in an ultrasonic bath using ethanol for a duration of 10 minute. After completing the initial cleaning process, the ethanol was substituted with deionized water and the procedure was repeated. Finally, the substrates were dried with an air blower. Zinc acetate dihydrate was used as the starting material. It was dissolved in ethanol, and a separate sodium hydroxide solution was prepared. The zinc acetate dihydrate solution was incrementally introduced into the sodium hydroxide solution at a flow rate of 1 ml per minute. This process occurred on a hot plate at 60 °C with stirring at 300 rpm. The substrate was annealed at 80 °C for 3 hour while adding 10 drops of zinc oxide solution. A niobium solution was prepared by dissolving zinc hydride and 1% mol niobium (1.32 mmol) within a mixture of ethanol, hexamethylenetetramine, and deionized water. The niobium solution was then deposited onto the substrates. This procedure was repeated for substrates with different growth durations at 100 °C.

2.3 Characterization

The comprehensive characterization of Nb-doped ZnO thin films involves several crucial analytical techniques to understand their morphological, crystallinity, optical, and electrical properties. Surface morphology analysis through SEM provides detailed insights into the film's surface features and grain structure at various magnifications, essential for understanding the impact of Nb doping on film formation. XRD analysis confirms the crystalline structure and phase composition, typically revealing a hexagonal wurtzite structure characteristic of ZnO films. The optical properties examined through UV-Vis spectroscopy are fundamental for evaluating the transparency and absorption characteristics of the film across the UV-visible spectrum, particularly important for photovoltaic applications. The inclusion of electrical characterization using the Keithley source meter enables the assessment of the film's conductivity and photoelectric response.

2.3.1 Morphology Properties

The morphological properties of Nb-doped ZnO were assessed using a Zeiss EVO 18 microscope at magnifications of 3000×, 5000×, and 8000×. This method enables the analysis of surface morphology and particle size distribution of Nb-doped ZnO by providing high-resolution images that clarify detailed surface features and particle shapes, resulting in an effective technique for morphology analysis.

2.3.2 Crystanility Properties

The crystalline structure and phase purity were measured using the Rigaku Miniflex 600, along with the PANalytical X'PERT PRO software, which also assesses the impact of Nb doping on the hexagonal structure of ZnO. To maximize the performance in applications of the material such as luminescent downshifting layers, these methods provide a comprehensive grasp of its structural characteristics.

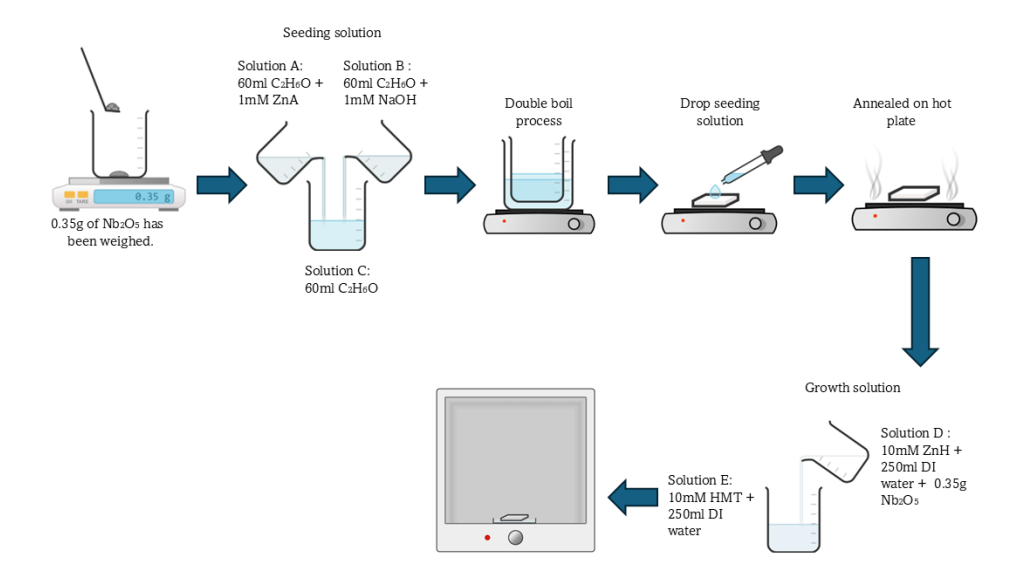


Fig 1. The schematic synthesis of Nb-doped ZnO as the luminescent downshifting layer.

$$d = \frac{K \lambda}{\beta \cos \theta} \tag{1}$$

The average size of the crystallites was determined by applying the Debye-Scherrer equation, where λ represents the wavelength of the X-ray, β represents the corrected full width at half maximum (FWHM) in radians, θ represents the Bragg angle in degrees, and K represents the Scherrer constant. The value of K is influenced by several parameters including crystal morphology, diffraction line indices, and the dispersion of crystallite sizes in the powder. In general, the value of K falls within the range of 0.62 to 2.08 (Uvarov *at el.*, 2013), often ranging from 0.9 to 1 for spherical particles or in cases when the shape of the crystallite is not known (Hassanzadeh *et el.*, 2023; He *et al.*, 2004).

2.3.3 Optical Properties

The optical properties are analyzed through UV-Vis (Shimadzu 1800) spectroscopy, elucidating the absorption characteristics and the bandgap of the bandgap. This information is essential for comprehending light absorption and optimizing layers during the simulation phase.

2.3.4 Electrical Properties

Using a Keithley 2401 source meter is used via 2-probe method for the electrical characterization on the growth Nb-doped ZnO layer. The average resistivity, average conductivity of the samples, and sheet resistance have been measured to further understand the charge carrier mechanism.

3. Results and Discussion

3.1 Morphology Properties

The morphological characteristics of ZnO nanoparticles on thin films were examined using SEM. As depicted in Figure 2, the SEM images reveal the structural features of ZnO nanoparticles

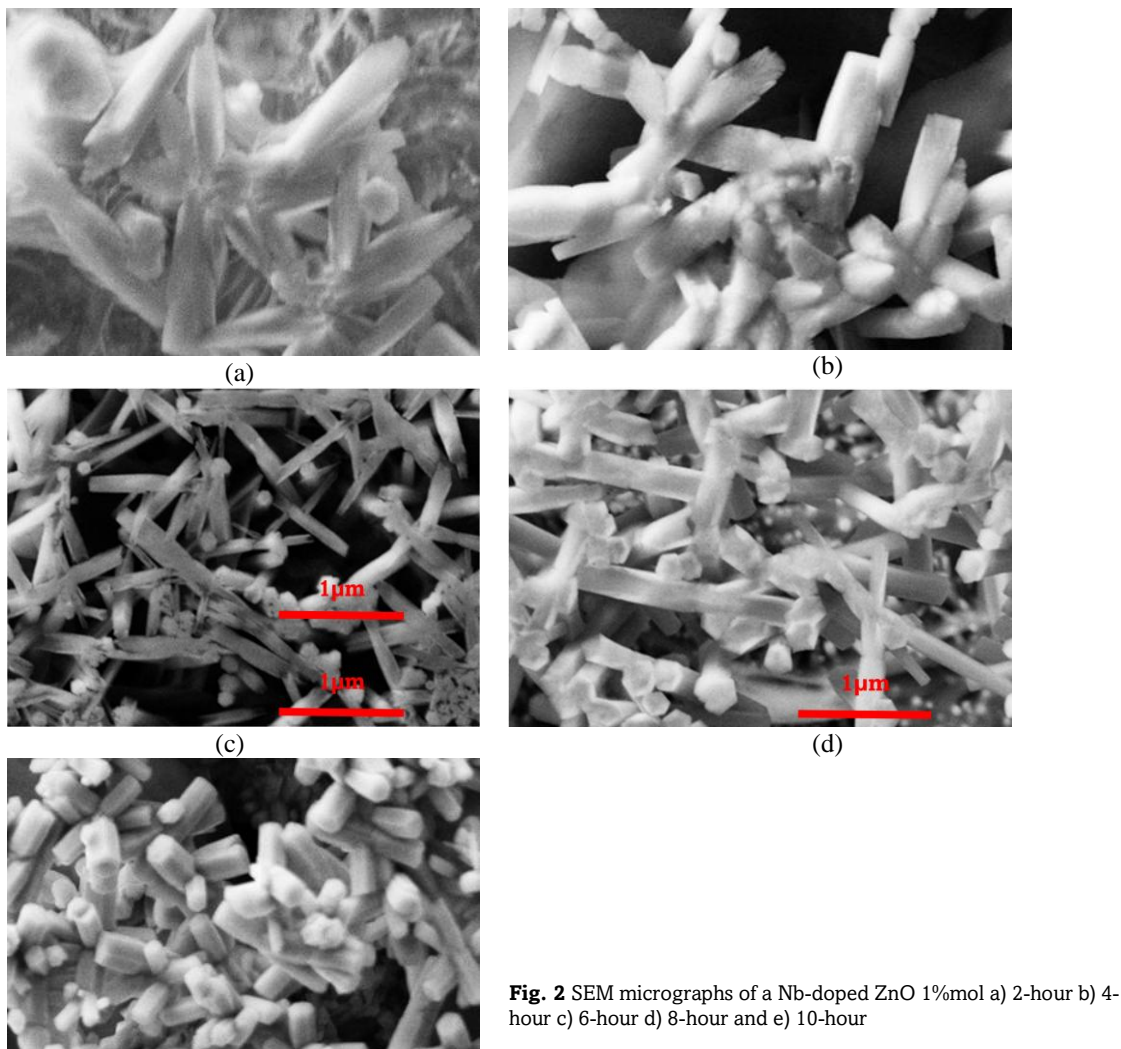
that were deposited onto thin films via the hydrothermal method. These nanoparticles were synthesized using a consistent dopant mass ratio but with varying growth durations. The images provide a visual representation of how the growth time influences the morphology of the ZnO nanostructures while maintaining a constant dopant concentration.

The experiments conducted involved the synthesis of ZnO nanostructures over varying growth periods of 2, 4, 6, 8, and 10 hours. Despite the irregular orientation and diverse aspect ratios observed, all crystallites consistently exhibited a hexagonal prismatic form, characteristic of ZnO nanostructures (Fudzi et al., 2018) mark, the growth process proceeded at a relatively slow pace. This can be attributed to the low reaction kinetics at 100 °C, which resulted in a gradual ZnO precipitation and limited particle density formation (Uvarov *et al.*, 2007). The initial stage of nanostructure development was thus characterized by this slower growth rate.

As shown in Figure 2(c & d), after 6 and 8 hours of the hydrothermal method, the nanoparticles began to change into a spherical shape and started to aggregate into rod-like structures. Figure 2(e) illustrates that the ZnO nanorods formed are inhomogeneous and randomly oriented. When the growth time of the nanostructures was extended to 10 hour, dense nanorods were observed, indicating a depletion of Zn ions by the end of the growth process (Fudzi et al., 2018). Hydrothermal synthesis is a straightforward and effective technique for crystallizing materials when they are deionized in a solution. By utilizing an appropriate synthesis architecture, the hydrothermal method can successfully produce one-dimensional nanorods as demonstrated above (Uvarov et al., 2007). The yield of the endothermic reaction during this process is influenced by the rates of nucleation and crystal growth (Uvarov et al., 2007).

3.2 Crystanility Properties

X-ray diffraction (XRD) examination was performed to evaluate the crystallinity and characteristics of the Nb-doped ZnO synthesized with varying growth durations. The pattern in Figure 3 shows crystal planes of (100), (002), (101), (102), (103)



and (202), which correspond well with diffraction peaks of 31.51°, 34.19°, 36.53°, 44.07°, 64.20° and 77.25° respectively.

(e)

The XRD pattern of Nb-doped ZnO nanoparticles shows diffraction peaks at 36.53° indicating the presence of the Nb phase and confirming Nb (V) in the ZnO matrix (Uvarov et al., 2007; Uvarov et al., 2013). The strong peak intensity at 2θ = 36.53° indicates that highly crystalline, which at this particular molarity, it is possible to produce c-axis orientated Nb-doped ZnO thin films (Mohd Fudzi et al., 2018; Tan et al., 2021). The JCPDS file number 00-036-1451 indicates that the diffraction peaks correspond to the hexagonal wurtzite structure of the ZnO crystal with cell constants of a = 0.3249 nm and c = 0.5206nm (Li et al., 2008).

Table 1 presents crystallite size changed over time as growing time increased for samples containing 1% Nb. XRD research demonstrated a consistent pattern in crystallite size development throughout different growth stages. Initially, at 2 hours of development time, the crystallite size was measured at 45.3 nm, indicating the biggest crystallite formation. As the growth time increased, the crystallite size gradually decreased, reaching 41.62 nm at 4 hours and 39.42 nm at 6 hours. After 8 hours, the crystallite size had decreased to 37.18 nm, its lowest point. However, after 10 hours of growth, there was a modest increase to 38.33 nm.

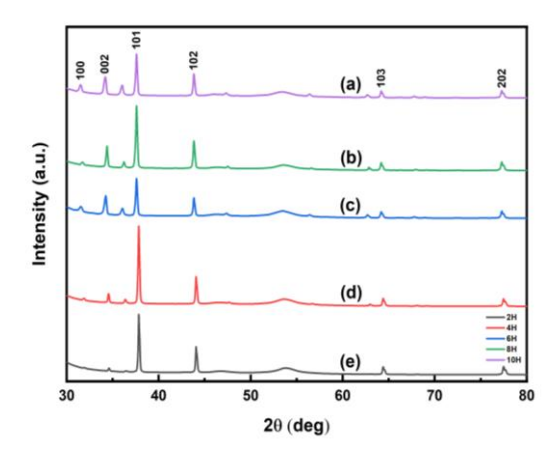


Fig. 3 X-ray diffraction spectra of ZnO doped with Nb for various growth durations: (a) 2 hour, (b) 4 hour, (c) 6 hour, (d) 8 hour, and (e) 10 hour.

Table 1The crystallite size with different growth hour of 1%mol Nb-doped ZnO thin films concentration.

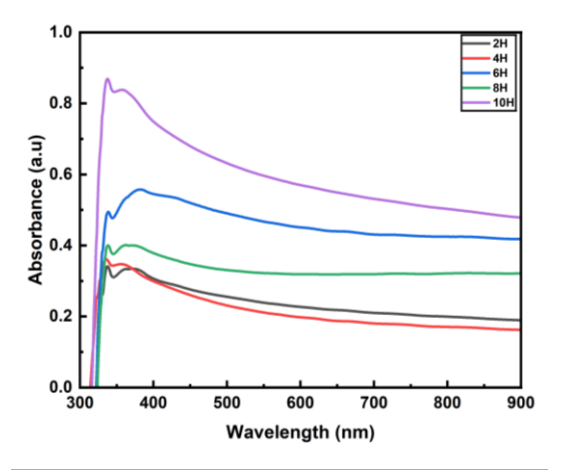
Nb Content (%)	Growth Hour (H)	Crystallite Size (nm)
-	2	45.3
	4	41.62
1%	6	39.42
	8	37.18
	10	38.33

Therefore, the crystallite size increased by approximately 3.09% from 8 hours (37.18 nm) to 10 hours (38.33 nm) of growth time. This relatively small percentage increase supports crystal agglomeration occurs through a dynamic process where particles can break and recombine, leading to size variations over time (Rodenbücher *et al.*, 2016). This process can result in both size reduction and occasional increases in particle dimensions. Additionally, the growth kinetics in doped systems show that Nb dopants are typically distributed in a statistically random manner, which can influence the crystal growth and recrystallization behaviour (Maghsoodi *et al.*, 2014).

3.3 Optical Properties

Figure 4 depicts the absorbance of Nb-doped ZnO at different growth hours. The UV-Vis absorption properties of the thin films were evaluated across a wavelength range of 300 to 900 nm. All thin films had absorption margins at 320 nm. By extending the growth time from 6 to 10 hour, the absorption edge displayed a red shift, indicating a reduction in the width of the energy gap between the conduction band (C_B) and the valence band (V_B) (Ananda *et al.*, 2014; Tan *et al.*, 2021).

Figure 5 illustrates that thin films demonstrate elevated transmittance in the visible spectrum while exhibiting reduced transmittance in the ultraviolet spectrum. The 2-hour sample exhibits the highest transmittance, which declines from approximately 65% to 45%. The observed reduction can be attributed to improved scattering effects in Nb-doped ZnO thin films on a PET substrate (Abdulrahman *et al.*, 2018). The incorporation of Nb ions into the ZnO lattice leads to the



 ${\bf Fig.4}$ Absorbance spectra of the Nb-doped ZnO thin films varied with different growth hours

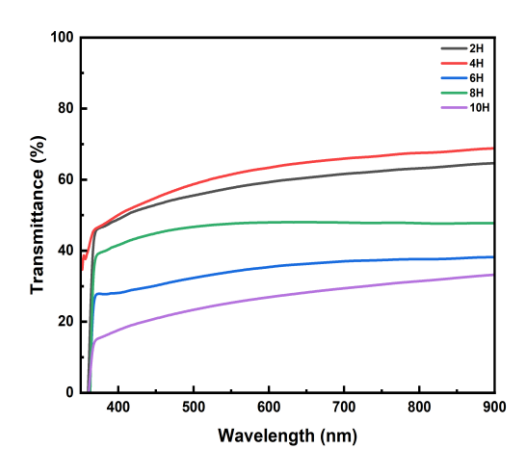


Fig.5 Transmittance of Nb-doped ZnO with different growth

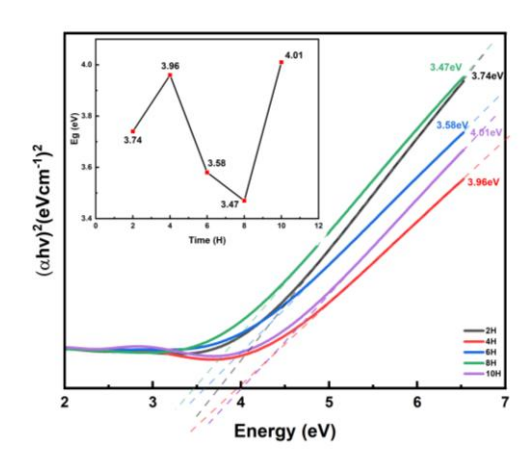


Fig.6 The plots of $(\alpha h v)^2$ versus energy and the inset is E_g for the Nb-doped ZnO thin films.

creation of oxygen vacancies and intrinsic defects, particularly at reduced concentrations. These defects act as scattering centres, thus reducing optical transparency (Ikram *et al.*, 2022). The topography of the substrate, the thickness of ZnO nanorods, and the morphology of the nanorods can all influence optical scattering, resulting in reduced transmittance of ZnO nanorod thin films (Abdulrahman *et al.*, 2018).

Based on Figure 6 the corresponding band gap at 2 hours, 4 hours, 6 hours, 8 hours and 10 hours were 3.74 eV, 3.96 eV, 3.58 eV, 3.47 eV, and 4.01 eV respectively. The minimum and maximum energy band gap is noted on Nb-doped ZnO on 8 hours and 10 hour samples. Although the trend deviates from the expected behavior for optical bandgap, the addition of Nb dopants resulted in a bandgap expansion from 3.37 eV (Tan *et al.*, 2021; Uvarov *et al.*, 2007) to 4.01 eV. This could be due to surface effects, particularly defects introduced during prolonged growth. These defects might increase the electron transition barrier, leading to a further widening of the bandgap (Liu *et al.*, 2019).

The Burstein-Moss Effect indicates that with an increase in Nb concentration (Ikram *et al.*, 2022), the optical bandgap rises from 3.37 to 4.01 eV. This phenomenon occurs as excess free

electrons fill the lower levels of the conduction band, resulting in a higher Fermi level (Saw *et al.*, 2015). The band filling effect occurs when Nb serves as a donor in ZnO, leading to the introduction of states above the conduction band minimum, which results in the Fermi level shifting into the conduction band. This results in the occupation of the lowest states of the conduction band by an excess free electron.

3.3 Electrical Properties

The graph demonstrates on Figure 7 the inverse correlation between average electrical conductivity and resistivity of Nb-doped ZnO across varying growth durations ranging from 2 to 10 hours. During the initial 2–4-hour period, conductivity remains relatively stable at approximately 1.4×10^{-3} , whereas resistivity exhibits a notable reduction from 1.4×10^{3} to 7.5×10^{2} Ω . At 6 hours, both properties exhibit moderate values, with conductivity decreasing to 1.2×10^{-3} . The system attains optimal electrical properties at 8 hours, with conductivity peaking at 1.55×10^{-3} and exhibiting relatively low resistivity. At 10 hours, a notable change is observed, with conductivity decreasing to 6.8×10^{-4} and resistivity increasing to 1.8×10^{3} Ω , indicating a significant transition in the electrical properties of the material over prolonged growth periods.

The 8-hour sample demonstrates the lowest bandgap of 3.47 eV and the highest conductivity of 1.54×10^{-3} S/cm. This inverse relationship is characteristic of semiconductors, wherein a reduced band gap facilitates electron transition from the valence band to the conduction band, thereby increasing conductivity. The improvement is due to the generation of electrons and

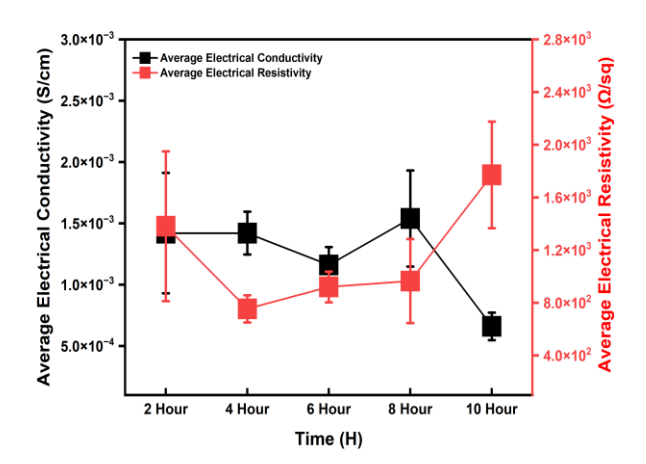


Fig.7 Average electrical conductivity and resistivity of Nb-doped ZnO samples at different growth hours.

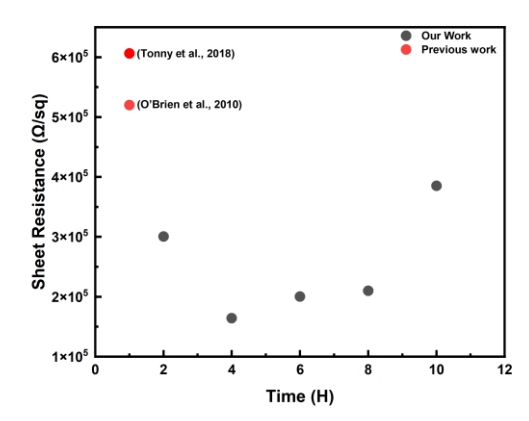


Fig.8 Sheet resistance of Nb-doped ZnO thin films measured at various sample distances.

donor states within the ZnO bandgap, which together enhance conductivity (Kumar *et al.*, 2017).

Furthermore, the resistivity graph illustrates a non-linear relationship with exposure time. Resistivity initially decreases from 2 to 4 hours, followed by a gradual increase until 8 hours, and then experiences a sharp rise at 10 hours. The presence of donor levels in Nb-doped ZnO thin films contributes to the observed reduction in resistivity between 2 and 4 hours (Zheng *et al.*, 2016). The notable rise in resistivity observed at 10 hours is ascribed to Nb doping, leading to a considerable improvement in conductivity by multiple orders of magnitude (Mostafa *et al.*, 2024).

The sheet resistance of the Nb-doped ZnO thin films developed in this study shows notable differences compared to findings from earlier studies (O'Brien et al., 2010; Tonny et al., 2018). As illustrated in Figure 8, the sheet resistance of the Nb-doped ZnO thin films is generally lower than that of both bare ZnO (O'Brien *et al.*, 2010) and Al-doped ZnO (Tonny *et al.*, 2018) within the measured time frame. The sample taken at four hours exhibited the lowest sheet resistance at $163.906 \times 10^3 \,\Omega/sq$.

Both optical transparency and sheet resistance are critical parameters for metal oxide-based transparent conductive electrodes (TCEs), which are vital for solar cell applications (Anand *et al.*, 2021; Ivanova *et al.*, 2022). While the influence of sheet resistance may be subtle and less straightforward, it plays a significant role in the overall performance of the device (Anand *et al.*, 2021; Ivanova *et al.*, 2022).

Based on Table 2 Nb-doped ZnO exhibits significant potential as a luminescent down-shifting layer, efficiently converting UV-blue photons into visible light to improve solar cell efficiency (Zhu n.d.). The material exhibits optimal properties at a growth duration of 8 hours, characterized by a bandgap of 3.35 eV, which is closest to the ideal ZnO. It also

Table 2Characterization parameters of control and Nb-doped ZnO sample with different growth hour

<u> </u>	Control comple	2H	4H	6H	8H	10H
	Control sample	ΖП	4П	ОП	оп	10П
	(Ismail et al., 2016)					
Absorbance	-	0.223	0.201	0.45	0.33	0.561
Bandgap (eV)	3.3	3.79	4.05	3.67	3.35	5.47
Crystallite size (nm)	30.7	45.3	41.62	39.42	37.18	38.33
Conductivity (S/cm) ×10 ⁻³	-	1.42	1.26	1.18	1.62	0.66
Resistivity (k Ω cm) ×10 ³	-	1.38	2.53	0.89	0.95	1.77
Sheet resistance (Ω/sq) ×10 ³	-	300	163.9	200.153	209.758	385.093

demonstrates a moderate transmittance of 46.54% and a peak conductivity of 1.62×10^{-3} S/cm, facilitating efficient photon conversion. The doping modification from the control sample E_g =3.3 eV to enhanced bandgap values range 3.35 to 5.47 eV indicates successful incorporation of Nb. Additionally, the decreased transmittance from 63.85% to 26.35% at 10H suggests improved UV absorption capability (Bazzari et al. 2020). The evolution of crystallite size from 30.7 nm in the control sample to 45.3 nm at 2H, followed by a gradual decrease, alongside variations in electrical properties, indicates that Nb doping significantly alters the structural and optical characteristics of ZnO. This modification results in an effective down-shifting layer that enhances solar cell performance by improving UV light utilization (Apostoluk et al., 2013). Nb doping significantly modifies the optical, structural, and electrical properties in comparison to the control sample, with the 8-hour sample demonstrating optimal performance prior to degradation at extended growth durations.

4. Conclusion

This study concludes that Nb-doped ZnO shows significant potential as a luminescent down-shifting layer, especially with an 8-hour growth time, characterized by optimal electrical conductivity, a stable bandgap, and advantageous crystallite size. The material efficiently converts UV-blue photons into visible light, thereby improving its applicability in solar cell technologies. The notable changes in optical, structural, and electrical properties relative to undoped ZnO underscore the potential of Nb doping. Nb-doped ZnO thin films were synthesized using a cost-effective hydrothermal method. The synthesis parameters, particularly growth temperature, significantly influenced the morphology, crystallinity, and optical properties. The bandgap ranged from 3.47 to 4.01 eV, exhibiting significant UV absorption in the 300-400 nm range and an average visible transmittance greater than 10%. Future research will concentrate on adjusting the molar concentration of Nb dopants to enhance these properties and investigate their full potential in photovoltaic devices. Future research on the luminescent downshifting layer of Nb-doped ZnO will examine different Nb concentrations and growth durations to elucidate the correlation between molar concentration and growth time.

Acknowledgments

This research is supported by grant ANTARABANGSA/RSC/2024/FKTEK/A00075 and Universiti Teknikal Malaysia, Melaka through the Kesidang Scholarship.

Author Contributions: Yaumee Natasha Jusoh: Conceptualization, methodology, formal analysis, writing—original draft, Faiz Arith; supervision, resources, project administration. All authors have read and agreed to the published version of the manuscript.

Funding: The author(s) received no financial support for the research, authorship, and/or publication of this article.

Conflicts of Interest: The authors declare no conflict of interest.

References

Abdulrahman, A. F., Ahmed, S. M., & Ahmed, N. M. (2018). Investigation of optical properties of ZnO nanorods grown on different

- substrates. *Science Journal of University of Zakho*, *6*(4), 160–165. https://doi.org/10.25271/SJUOZ.2018.6.4.546
- Alias, N. S. N. M., Arith, F., Mustafa, A. N. M., Mustafa, A. N. M., Ismail, M. M., Chachuli, S. A. M., & Shah, A. S. M. (2022). Compatibility of Al-doped ZnO electron transport layer with various HTLs and absorbers in perovskite solar cells. *Applied Optics, Vol. 61, Issue 15, Pp.* 4535-4542, 61(15), 4535-4542. https://doi.org/10.1364/AO.455550
- Alias, N. S. N. M., Arith, F., Mustafa, A. N., Ismail, M. M., Azmi, N. F., & Saidon, M. S. (2022). Impact of Al on ZnO Electron Transport Layer in Perovskite Solar Cells. *Journal of Engineering and Technological Sciences*, 54(4). https://doi.org/10.5614/j.eng.technol.sci.2022.54.4.9
- Aliyaselvam, O. V., Arith, F., Rong, I. J., Zin, S. I., Ali, F. A., & Mustafa, A. N. (2022). Facile Synthesis of Copper Iodide at Low Temperature as Hole Transporting Layer for Perovskite Solar Cell. *International Journal of Renewable Energy Research (IJRER)*, 12(2), 892–898. https://doi.org/10.20508/IJRER.V12I2.12825.G8473
- Anand, A., Islam, M. M., Meitzner, R., Schubert, U. S., & Hoppe, H. (2021). Introduction of a novel figure of merit for the assessment of transparent conductive electrodes in photovoltaics: Exact and approximate form. *Advanced Energy Materials*, 11(26), 2100875. https://doi.org/10.1002/aenm.202100875
- Ananda, S., Gowda, N. M. M., & Raksha, K. R. (2014). Synthesis of niobium doped ZnO nanoparticles by electrochemical method: characterization, photodegradation of indigo carmine dye and antibacterial study. Advances in Nanoparticles, 3(04), 133. https://doi.org/10.4236/anp.2014.34018
- Apostoluk, A., Zhu, Y., Canut, B., Masenelli, B., Delaunay, J. J., Znajdek, K., & Sibiński, M. (2013). Investigation of luminescent properties of ZnO nanoparticles for their use as a down-shifting layer on solar cells. *Physica Status Solidi (C) Current Topics in Solid State Physics*, 10(10), 1301–1307. https://doi.org/10.1002/PSSC.201200950
- Bagiyev, E., Balayeva, N., Aliyeva, Y., Kerimova, A., Valiyev, R., Mamiyev, Z., ... Bayramov, A. (2015). Optimization of preparation technology of ZnO and ZnO: Al thin films for solar cell applications. *Physica Status Solidi (c)*, 12(6), 536–539. https://doi.org/10.1002/PSSC.201400364
- Bazzari, H. H., Abushgair, K. N., Hamdan, M. A., & Alkhaldi, H. S. (2020). Cooling Solar Cells Using ZnO Nanoparticles as, Thermal Science 24(2A), 809–814. https://doi.org/10.2298/TSCI180324004B
- Cantarella, M., Spanò, V., Zimbone, M., Giuffrida, F., Lufrano, E., Strano, V., ... Impellizzeri, G. (2024). ZnO–MoS2-PMMA polymeric nanocomposites: A harmless material for water treatment. *Materials Today Chemistry*, 36, 101912. https://doi.org/10.1016/J.MTCHEM.2024.101912
- Chvostová, D., Dejneka, A., Hubička, Z., Churpita, A., Bykov, P., Jastrabík, L., & Trepakov, V. A. (2011). Synthesis and optical properties of Mn doped ZnO thin films. *Physica Status Solidi (a)*, 208(9), 2140–2143. https://doi.org/10.1002/pssa.201026630
- Çolak, H., Karaköse, E., & Sungür, Ç. (2023). Niobium doping effect on electrical and optical properties of ZnO nanorods produced by ultrasonic spray pyrolysis. *Physica B: Condensed Matter*, 671, 415455. https://doi.org/10.1016/J.PHYSB.2023.415455
- Dhawan, R., & Panda, E. (2019). Mg addition in undoped and Al-doped ZnO films: Fabricating near UV transparent conductor by bandgap engineering. *Journal of Alloys and Compounds*, 788, 1037–1047. https://doi.org/10.1016/J.JALLCOM.2019.02.289
- El Fakir, A., Sekkati, M., Schmerber, G., Belayachi, A., Edfouf, Z., Regragui, M., ... Slaoui, A. (2017). Influence of Rare Earth (Nd and Tb) Co-Doping on ZnO Thin Films Properties. *Physica Status Solidi c*, 14(10), 1700169. https://doi.org/10.1002/pssc.201700169
- Eswar, K. A., Mohamad, M., Akhir, R. M., Mashjur, I. N. Z., Zamri, N. Z., Rostan, N. F., ... Malek, M. F. (2023). Morphological and optical properties of Nb-doped ZnO nanoparticles. *Materials Today: Proceedings,* 75, 74–78. https://doi.org/10.1016/j.matpr.2022.10.081
- Fu, C. F., Han, L. F., Liu, C., & Gao, Y. F. (2013). Effects of Cr-doping concentration on the structural, optical, and magnetic properties of ZnO thin films. *Physica Status Solidi (a)*, 210(7), 1358–1362. https://doi.org/10.1002/PSSA.201329014

- Fudzi, L. M., Zainal, Z., Lim, H. N., Chang, S. K., Holi, A. M., & Ali, M. S. M. (2018). Effect of Temperature and Growth Time on Vertically Aligned ZnO Nanorods by Simplified Hydrothermal Technique for Photoelectrochemical Cells. *Materials (Basel, Switzerland)*, 11(5). https://doi.org/10.3390/MA11050704
- Gerbreders, V., Krasovska, M., Sledevskis, E., Gerbreders, A., Mihailova, I., Tamanis, E., & Ogurcovs, A. (2020). Hydrothermal synthesis of ZnO nanostructures with controllable morphology change. *CrystEngComm*, 22(8), 1346–1358. https://doi.org/10.1039/C9CE01556F
- Guzman, E., Hochmuth, H., Lorenz, M., von Wenckstern, H., Rahm, A., Kaidashev, E. M., ... Pöppl, A. (2004). Pulsed laser deposition of Fe-and Fe, Cu-doped ZnO thin films. *Annalen Der Physik*, 516(1–2), 57–58. https://doi.org/10.1002/andp.200451601-213
- Hammad, A. H., & Abdel-Wahab, M. S. (2021). Characterization of niobium-doped zinc oxide thin films: Structural changes and optical properties. *Materials Today Communications*, 26, 101791. https://doi.org/10.1016/j.mtcomm.2020.101791
- Hassanzadeh-Tabrizi, S. A. (2023). Precise calculation of crystallite size of nanomaterials: A review. *Journal of Alloys and Compounds*, 171914. https://doi.org/10.1016/j.jallcom.2023.171914
- He, J., Ye, J., Lavernia, E. J., Matejczyk, D., Bampton, C., & Schoenung, J. M. (2004). Quantitative analysis of grain size in bimodal powders by X-ray diffraction and transmission electron microscopy. *Journal of Materials Science*, 39, 6957–6964. https://doi.org/10.1023/B:JMSC.0000047538.95825.ad
- Ikram, M., Shahid, H., Haider, J., Haider, A., Naz, S., Ul-Hamid, A., ...
 Ali, S. (2022). Nb/Starch-Doped ZnO Nanostructures for Polluted
 Water Treatment and Antimicrobial Applications: Molecular
 Docking Analysis, 7, 39361.
 https://doi.org/10.1021/acsomega.2c05569
- Ismail, A. S., Mamat, M. H., Md Sin, N. D., Malek, M. F., Zoolfakar, A. S., Suriani, A. B., ... Rusop, M. (2016). Fabrication of hierarchical Sn-doped ZnO nanorod arrays through sonicated sol-gel immersion for room temperature, resistive-type humidity sensor applications. *Ceramics International*, 42(8), 9785–9795. https://doi.org/10.1016/J.CERAMINT.2016.03.071
- Ivanova, T., Harizanova, A., Koutzarova, T., Vertruyen, B., & Closset, R. (2022). Deposition of Sol–Gel ZnO:Mg Films and Investigation of Their Structural and Optical Properties. *Materials*, *15*(24). https://doi.org/10.3390/MA15248883
- Jafari, H., Sadeghzadeh, S., Rabbani, M., & Rahimi, R. (2018). Effect of Nb on the structural, optical and photocatalytic properties of Aldoped ZnO thin films fabricated by the sol-gel method. *Ceramics International*, 44(16), 20170–20177. https://doi.org/10.1016/J.CERAMINT.2018.07.311
- Jalaludin, N. A., Salehuddin, F., Rahim, F. L., Mustafa, A. N., Kaharudin, K. E., Islam, M. A., ... Arith, F. (2025). Efficient hole extraction by doped-polyaniline/graphene oxide in lead-free perovskite solar cell: a computational study. *Physica Scripta*, 100(2), 025924. https://doi.org/10.1088/1402-4896/ADA4E8
- Jusoh, Y. N., Arith, F., Khafe, A. M., Chachuli, S. A. M., Nor, M. K., Mustafa, A. N., & Salehuddin, F. (2024). Carrier Injection Mechanism of Nb-Doped ZnO Thin Films in Light Emission Properties. *Przeglad Elektrotechniczny*, (11), 95–98. https://doi.org/10.15199/48.2024.11.17
- Khalil, M. I., Al-Qunaibit, M. M., Al-zahem, A. M., & Labis, J. P. (2014). Synthesis and characterization of ZnO nanoparticles by thermal decomposition of a curcumin zinc complex. *Arabian Journal of Chemistry*, 7(6), 1178–1184. https://doi.org/10.1016/J.ARABJC.2013.10.025
- Khare, N., Kappers, M. J., Wei, M., Blamire, M. G., & MacManus-Driscoll, J. L. (2006). Defect-Induced Ferromagnetism in Codoped ZnO. Advanced Materials, 18(11), 1449–1452. https://doi.org/https://doi.org/10.1002/adma.200502200
- Kotlyarchuk, B., Savchuk, V., & Oszwaldowski, M. (2005). Preparation of undoped and indium doped ZnO thin films by pulsed laser deposition method. *Crystal Research and Technology*, 40(12), 1118– 1123. https://doi.org/10.1002/CRAT.200410502
- Kumar, R., Umar, A., Kumar, G., Nalwa, H. S., Kumar, A., & Akhtar, M. S. (2017). Zinc oxide nanostructure-based dye-sensitized solar cells. *Journal of Materials Science*, 52, 4743–4795. https://doi.org/10.1007/s10853-016-0668-z

- Li, Z., Huang, X., Liu, J., Li, Y., & Li, G. (2008). Morphology control and transition of ZnO nanorod arrays by a simple hydrothermal method. *Materials Letters*, 62(10–11), 1503–1506. https://doi.org/10.1016/J.MATLET.2007.09.011
- Liu, M., Zhan, Q., Li, W., Li, R., He, Q., & Wang, Y. (2019). Effect of Zn doping concentration on optical band gap of PbS thin films. Journal of Alloys and Compounds, 792, 1000–1007. https://doi.org/10.1016/j.jallcom.2019.04.117
- Lu, Y. M., Chang, C. M., Tsai, S. I., & Wey, T. S. (2004). Improving the conductance of ZnO thin films by doping with Ti. *Thin Solid Films*, 447–448, 56–60. https://doi.org/10.1016/J.TSF.2003.09.022
- Ma, L., Ai, X., Huang, X., & Ma, S. (2011). Effects of the substrate and oxygen partial pressure on the microstructures and optical properties of Ti-doped ZnO thin films. Superlattices and Microstructures, 50(6), 703-712. https://doi.org/10.1016/j.spmi.2011.09.012
- Maghsoodi, M., & Yari, Z. (2014). Effect of temperature on wet agglomeration of crystals. *Iran J Basic Med Sci*, *17*, 344–350. https://doi.org/10.22038/IJBMS.2014.2784
- Mohd Fudzi, L., Zainal, Z., Lim, H. N., Chang, S.-K., Holi, A. M., & Sarif@ Mohd Ali, M. (2018). Effect of temperature and growth time on vertically aligned ZnO nanorods by simplified hydrothermal technique for photoelectrochemical cells. *Materials*, 11(5), 704. https://doi.org/10.3390/ma11050704
- Mostafa, S., Besisa, D. H. A., Zahran, F., Ahmed, A., Elwan, M., Khalifa, A., & Ewais, E. M. M. (2024). Processing and enhancement of thermoelectric performance of Nb doped ZnO (NZO) ceramics. *Ceramics International*, 50(4), 6557–6566. https://doi.org/10.1016/J.CERAMINT.2023.11.403
- Mustaffa, M. A., Arith, F., Noorasid, N. S., Zin, M. S. I. M., Leong, K. S., Ali, F. A., . . . Ismail, M. M. (2022). Towards a Highly Efficient ZnO Based Nanogenerator. *Micromachines 2022, Vol. 13, Page 2200*, 13(12), 2200. https://doi.org/10.3390/MI13122200
- Naz, H., Ali, R. N., Liu, Q., Yang, S., & Xiang, B. (2018). Niobium doped zinc oxide nanorods as an electron transport layer for highperformance inverted polymer solar cells. *Journal of Colloid and Interface Science*, 512, 548–554. https://doi.org/10.1016/J.JCIS.2017.10.041
- Nguyen, T. H. A., Doan, V.-D., Tran, A. V., Nguyen, V. C., Nguyen, A.-T., & Vasseghian, Y. (2022). Green synthesis of Nb-doped ZnO nanocomposite for photocatalytic degradation of tetracycline antibiotic under visible light. *Materials Letters*, 308, 131129. https://doi.org/10.1016/j.matlet.2021.131129
- O'Brien, S., Nolan, M. G., Çopuroglu, M., Hamilton, J. A., Povey, I., Pereira, L., ... Pemble, M. (2010). Zinc oxide thin films: Characterization and potential applications. *Thin Solid Films*, 518(16), 4515–4519. https://doi.org/10.1016/j.tsf.2009.12.020
- Özgür, M., Pat, S., Mohammadigharehbagh, R., Musaoğlu, C., Demirkol, U., Elmas, S., ... Korkmaz, Ş. (2019). Sn doped ZnO thin film deposition using thermionic vacuum arc technique. *Journal of Alloys and Compounds*, 774, 1017–1023. https://doi.org/10.1016/J.JALLCOM.2018.10.020
- Pascariu, P., Homocianu, M., Cojocaru, C., Samoila, P., Airinei, A., & Suchea, M. (2019). Preparation of La doped ZnO ceramic nanostructures by electrospinning–calcination method: Effect of La3+ doping on optical and photocatalytic properties. Applied Surface Science, 476, 16–27. https://doi.org/10.1016/J.APSUSC.2019.01.077
- Rodenbücher, C., Luysberg, M., Schwedt, A., Havel, V., Gunkel, F., Mayer, J., & Waser, & R. (2016). Homogeneity and variation of donor doping in Verneuil-grown SrTiO 3:Nb single crystals. Nature Publishing Group. https://doi.org/10.1038/srep32250
- Sanz, O., Haro-Poniatowski, E., Gonzalo, J., & Fernández Navarro, J. M. (2006). Influence of the melting conditions of heavy metal oxide glasses containing bismuth oxide on their optical absorption. Journal of Non-Crystalline Solids, 352(8), 761–768. https://doi.org/10.1016/J.JNONCRYSOL.2006.02.002
- Saw, K. G., Aznan, N. M., Yam, F. K., Ng, S. S., & Pung, S. Y. (2015). New Insights on the Burstein-Moss Shift and Band Gap Narrowing in Indium-Doped Zinc Oxide Thin Films. https://doi.org/10.1371/journal.pone.0141180
- Tan, H. J., Zainal, Z., Talib, Z. A., Lim, H. N., Shafie, S., Tan, S. T., ... Bahrudin, N. N. (2021). Synthesis of high quality hydrothermally grown ZnO nanorods for photoelectrochemical cell electrode.

- Ceramics International, 47(10), 14194–14207. https://doi.org/10.1016/J.CERAMINT.2021.02.005
- Tonny, K. N., Rafique, R., Sharmin, A., Bashar, M. S., & Mahmood, Z. H. (2018). Electrical, optical and structural properties of transparent conducting Al doped ZnO (AZO) deposited by sol-gel spin coating. *AIP Advances*, 8(6). https://doi.org/10.1063/1.5023020
- Uvarov, V., & Popov, I. (2007). Metrological characterization of X-ray diffraction methods for determination of crystallite size in nanoscale materials. *Materials Characterization*, *58*(10), 883–891. https://doi.org/10.1016/j.matchar.2013.09.002
- Uvarov, Vladimir, & Popov, I. (2013). Metrological characterization of X-ray diffraction methods at different acquisition geometries for determination of crystallite size in nano-scale materials. *Materials*

- *Characterization*, 85, 111–123. https://doi.org/10.1016/j.matchar.2013.09.002
- Wahab, Z. A., Jalaludin, N. A., Nor, M. K., Mustafa, A. N. M., Shah, A. S. M., Salehuddin, F., & Arith, F. (2024). Insights of MoO3 HTL in Perovskite Solar Cells from a Simulation Perspective. *International Journal of Nanoelectronics and Materials (IJNeaM)*, 17, 31–38. https://doi.org/10.58915/IJNEAM.V17IDECEMBER.1604
- Zheng, X., Gao, F., Ji, F., Wu, H., Zhang, J., Hu, X., & Xiang, Y. (2016). Cu-doped PbS thin films with low resistivity prepared via chemical bath deposition. *Materials Letters*, 167, 128–130. https://doi.org/10.1016/J.MATLET.2015.12.077
- Zhu, Y. ZnO nanoparticles as a luminescent down-shifting layer for solar cells. SPIE. https://doi.org/10.1117/2.1201212.004585



© 2025. The Author(s). This article is an open access article distributed under the terms and conditions of the Creative Commons Attribution-ShareAlike 4.0 (CC BY-SA) International License (http://creativecommons.org/licenses/by-sa/4.0/)